NANO LETTERS

2005
Vol. 5, No. 7
1247−1253

Controllable Template Synthesis of Superconducting Zn Nanowires with Different Microstructures by Electrochemical Deposition

Jin-Guo Wang,* Ming-Liang Tian,† Nitesh Kumar,† and Thomas E. Mallouk‡

Materials Research Institute and Center for Nanoscale Science, Department of Physics, and Department of Chemistry, The Pennsylvania State University, University Park, Pennsylvania 16802

Received May 17, 2005; Revised Manuscript Received June 9, 2005

ABSTRACT

A systematic study was conducted on the fabrication, structural characterization, and transport properties of Zn nanowires with diameters between 40 and 100 nm. Zinc nanowires were fabricated by electrodepositing Zn into commercially available polycarbonate (PC) or anodic aluminum oxide (AAO) membranes. By controlling the electrodeposition process, we found that the nanowires can be single-crystal, polycrystalline Zn, crystalline Zn/nanocrystalline ZnO composites, or entirely ZnO. The microstructure and chemistry was characterized by using transmission electron microscopy. Transport studies on single-crystal or polycrystalline Zn nanowire arrays embedded inside the membrane showed that the superconducting transition temperature, T_c, is insensitive to the nanowire diameter and morphology. The superconductivity shows a clear crossover from bulklike to quasi-1D behavior, as evidenced by residual low-temperature resistance, when the diameter of the wires is reduced to 70 nm (20 times smaller than the bulk coherence length).

Confined systems of nanometer dimensions represent one of the important frontiers in advanced materials research. Because of their restricted size, these structures exhibit novel physical[1−4] and chemical[5] properties and have opened up a new area of basic research as well as possible applications in nanodevices. In the area of superconductivity, when the sample size becomes comparable to or smaller than the temperature-dependent coherence length, ξ (T), the properties of a superconductor are expected to change significantly.[6,7] Although experimental studies have been made on Sn,[8,9] Pb,[9,10] MoGe,[6] and Nb[11] nanowires in recent years, there are still controversies on what the expected properties of a 1D superconductor are. The main reason for the uncertainty is the broad range of microstructures, morphologies, and topologies of the samples used in the experiments. The contrasting results found in granular,[12] polycrystalline,[11] and amorphous wires[6,13−15] fabricated by sputtering or evaporation techniques make it difficult to conclude which, if any, of the observed effects is a direct consequence of 1D confinement.

Bulk zinc (Zn) is a conventional type-I superconductor with a transition temperature of 0.85 K (at $H = 0$ Oe) and a critical magnetic field of 50 Oe (at $T = 0$ K). More importantly, the superconducting coherence length of bulk Zn in clean limit, ξ_0, was reported to be 1.5−2.2 μm,[16] which is almost an order larger than those of the other materials mentioned above. Therefore, one-dimensional (1D) effects in Zn nanowires are expected to be more apparent compared to other wires of the same diameter. Fabrication of Zn nanowires,[17,18] nanofibers,[19] and nanobelts[20] has been reported previously by solid−vapor phase reaction, chemical etching, and other techniques. Metal-semiconductor Zn−ZnO core-shell nanobelts and nanotubes have also been synthesized mostly by solid−vapor phase reactions.[18,21−25]

Template synthesis (by electrochemical deposition) is a versatile and particularly simple approach, especially in the preparation of metallic nanowires.[26] Arrays of nanowires are obtained by filling a porous template that contains a large number of straight cylindrical holes with a controllable narrow size distribution. The morphology and microstructures of the nanowires fabricated by this technique can be controlled by tuning the deposition parameters, such as temperature, pH value, additives, and deposition potential.[26−28] Two types of commercially available templates, "track-etched" polycarbonate (PC) and anodic aluminum oxide (AAO) membranes, are usually used in the fabrication. The channels of pores in these membranes are aligned almost parallel to each other and perpendicular to the surface of the membrane without interconnections between adjacent pores. The pore density of an AAO membrane is about 10^{10}−

* To whom correspondence should be addressed: Dr. Jinguo Wang, The Pennsylvania State University, Materials Research Institute and The Center for Nanoscale Science, 194 MRI Building, University Park, PA 16802; e-mail: jqw11@psu.edu.

† Department of Physics and The Center for Nanoscale Science.

‡ Department of Chemistry and The Center for Nanoscale Science.

10.1021/nl050918u CCC: $30.25
Published on Web 06/21/2005

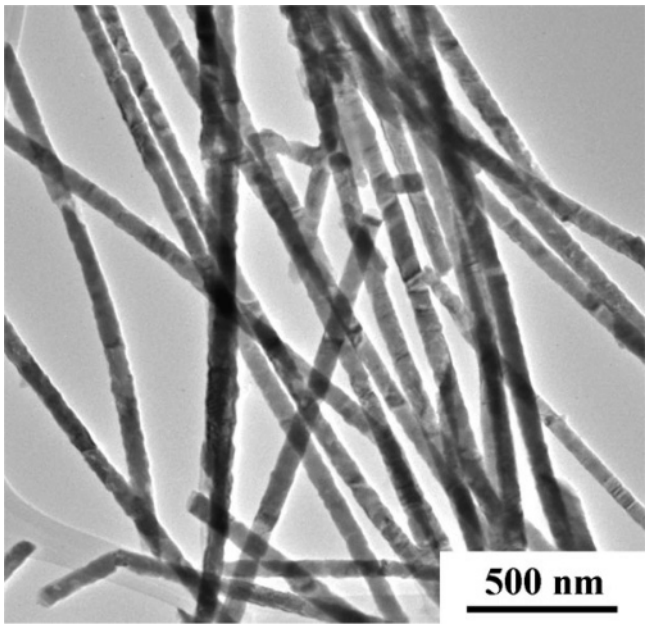

Figure 1. Low magnification TEM image of single-crystal Zn nanowires synthesized under 19 °C and $V = -0.7$ V.

10^{11} pores/cm^2, whereas for a PC membrane, the pore density is about 6×10^8 pores/cm^2, 2 orders of magnitude lower than that of AAO. Because the as-deposited nanowires embedded inside the membrane are well protected from oxidation, this makes transport measurements possible by attaching metal leads on both sides of the membrane.

In this paper we present a systematic study of the fabrication, structural characterization, and transport properties of Zn nanowires with diameters between 40 and 100 nm. We find that these nanowires can be single-crystal, polycrystalline Zn, crystalline Zn/nanocrystalline ZnO composites, or entirely ZnO and that the nature of the product can be controlled by adjusting the deposition conditions (deposition voltage, temperature, or additives). Transport studies on single-crystal and polycrystalline Zn nanowire arrays embedded inside the membranes show that the superconducting transition temperature, T_c, is insensitive to the sample diameter and morphology. However, the superconductivity shows a clear crossover from bulklike to quasi-1D behavior when the diameter of the wires is reduced to 70 nm (20 times smaller than the bulk coherence length).

Zinc nanowires were fabricated by electrodepositing Zn into commercially available PC or AAO membranes.[29−32] The electrolyte was prepared by mixing 200 mL of 0.18 M $ZnCl_2$ aqueous solution with 40 mL of saturated KCl and 0.5 g of gelatin. Prior to electrodeposition, a 200-nm Au film was evaporated onto one side of the membrane to serve as the conducting cathode lead. A pure Pt wire was used as the anode lead. Four different conditions are employed for electrochemical deposition (V_{SCE}: standard deposition potential vs saturated calomel electrode; T: temperature): (i) $V_{SCE} = -0.7$ V, $T = 19$ °C; (ii) $V_{SCE} = -1.5$ V, $T = 19$ °C; (iii) $V_{SCE} = -0.7$ V, $T = 75$ °C; (iv) $V_{SCE} = -1.5$ V, $T = 75$ °C. The nanowires were harvested by dissolving the PC membrane in dichloromethane or dissolving AAO with 5 M NaOH solution and were separated from the solvent by means of centrifugation. The free-standing nanowires were

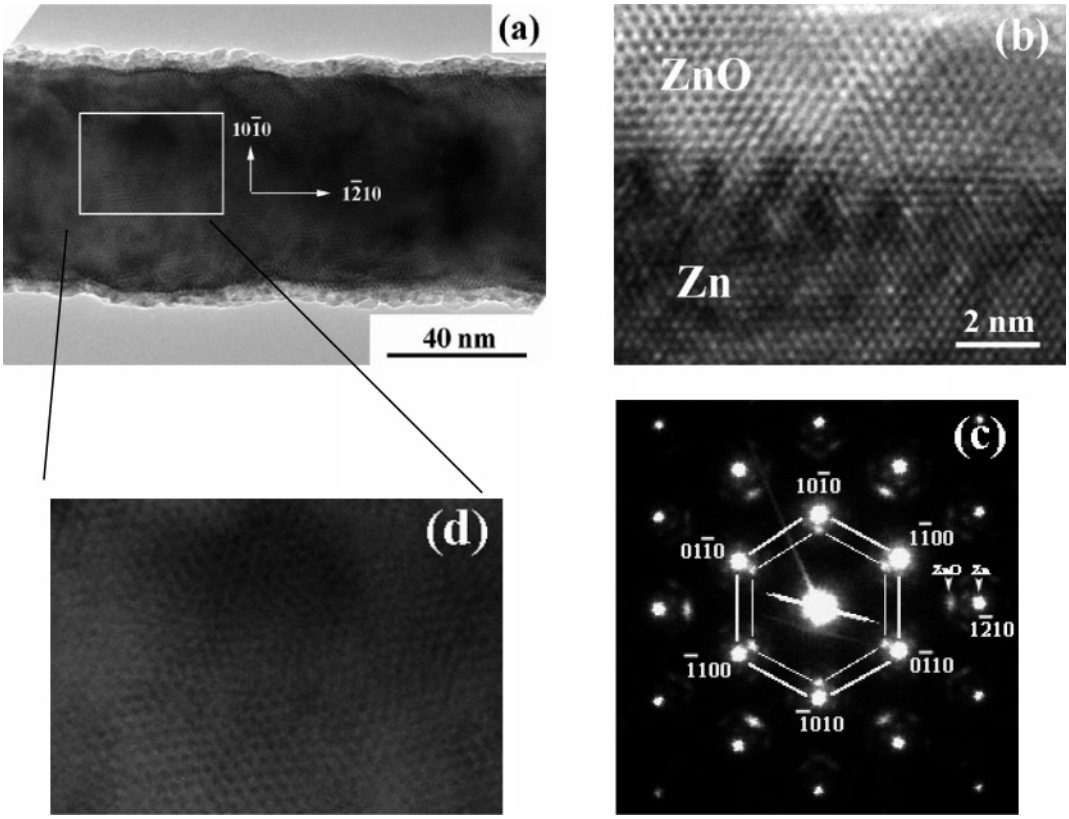

Figure 2. (a) Single-crystal nanowire growing along the $[1\bar{2}10]$ direction, in which the electron beam direction is parallel to $[0001]_{Zn}$, (b) local enlarged HREM image of the interface between Zn and ZnO, (c) select area electron diffraction patterns, and (d) moiré patterns on the surface of the nanowire.

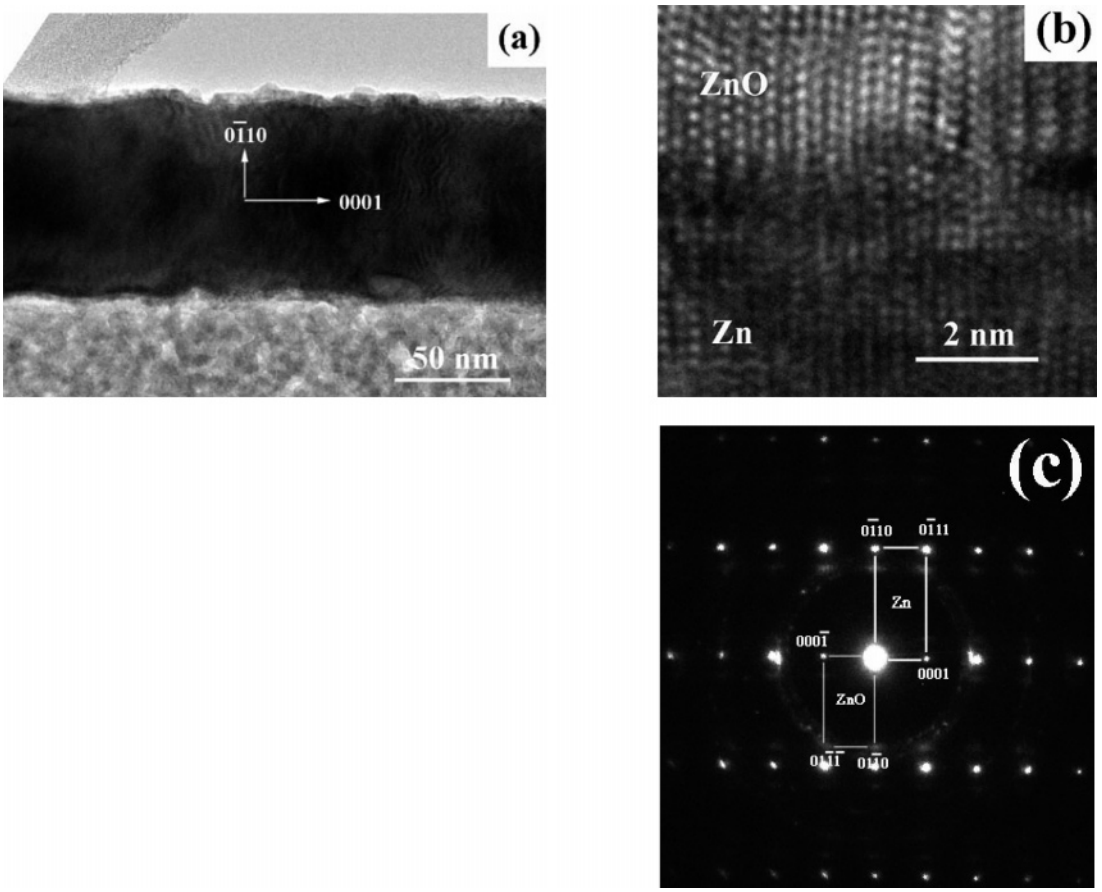

Figure 3. (a) Single-crystal nanowire growing along the [0001] direction, with the electron beam direction parallel to $[2\bar{1}\bar{1}0]_{Zn}$, (b) local enlarged HREM image of the interface between Zn and ZnO, and (c) select area electron diffraction patterns.

stored as a suspension in ethyl alcohol. The microstructures of the resulting nanowires were characterized by 200 kV JEOL 2010F field-emission transmission electron microscopy (FETEM), equipped with an annular dark field detector, a postcolumn electron energy loss (EELS) image (Gatan Enfina), and an Oxford energy-dispersive X-ray (EDX) detector. High-resolution TEM images and EDX analysis were used to identify the oxide phases in the nanowires, and the duration of the EDX scans on individual spots was 20−40 s. Transport measurement was made with the Physical Properties Measurement System (PPMS) (Quantum Design Inc.) equipped with a He3 cryostat so that the temperature could go down 0.45 K.

Figure 1 shows a bright-field low magnification FETEM image of Zn wires, deposited under condition i, namely, low temperature and low deposition potential. Because the nanowire was undergoing a centrifugation process before it was put on the TEM grid, some of the wires might show bend contours. The nanowires showed a single-crystalline structure with a uniform diameter of 70 nm. Checking individual wires in detail, we found that more than 95% of them were single-crystal along their entire length. Three growth orientations, $[1\bar{2}10]$, $[0\bar{1}10]$, and [0001], were observed. An oxide layer of ZnO, which may form after the nanowires are released from the membrane, was found in all cases with typical crystallographic orientation to the Zn wire. Thus, the free-standing nanowires examined by FETEM show a Zn−ZnO core-shell structure. Shown in Figure 2 is a single-crystal Zn nanowire growing along the $[1\bar{2}10]$ direction, in which the electron beam direction is parallel to $[0001]_{Zn}$. The epitaxial relationships between Zn and the oxide layer ZnO, which could be determined by the selected area electron diffraction patterns from Figure 2c, are $[0001]_{Zn}//[0001]_{ZnO}$, $(1\bar{2}10)_{Zn}//(1\bar{2}10)_{ZnO}$. A locally enlarged HREM image of the interface between Zn and the ZnO layer is shown in Figure 2b. The epitaxial relationship is confirmed by this image. The mismatch dislocations at the Zn/ZnO interface and the defects (such as stacking faults) in the ZnO layer are expected because of the lattice mismatch between Zn and ZnO; the misfit between Zn and ZnO in this orientation is 21.6%. A close look at the edge of the nanowire shows that the ZnO layer is actually composed of many small domains with an epitaxial relationship to the Zn core. The moiré pattern that results from overlap of the surface ZnO layer and the Zn core can be clearly observed in Figure 2d. As is well-known, the moiré fringes are very sensitive to the relative rotation angles between the ZnO and Zn. The different orientations of moiré patterns in Figure 2d indicate that the domains in the ZnO layer have different rotation angles with respect to the lattice of Zn. The small rotation can also be verified in the diffraction pattern shown in Figure 2c, in which the diffraction spots of ZnO are elongated. Similar results were reported in a recent publication on the oxidation of Zn nanoparticles.[33] This suggests that the ZnO layer in the present study may be caused by the oxidation of the metallic nanowire after electrodeposition.

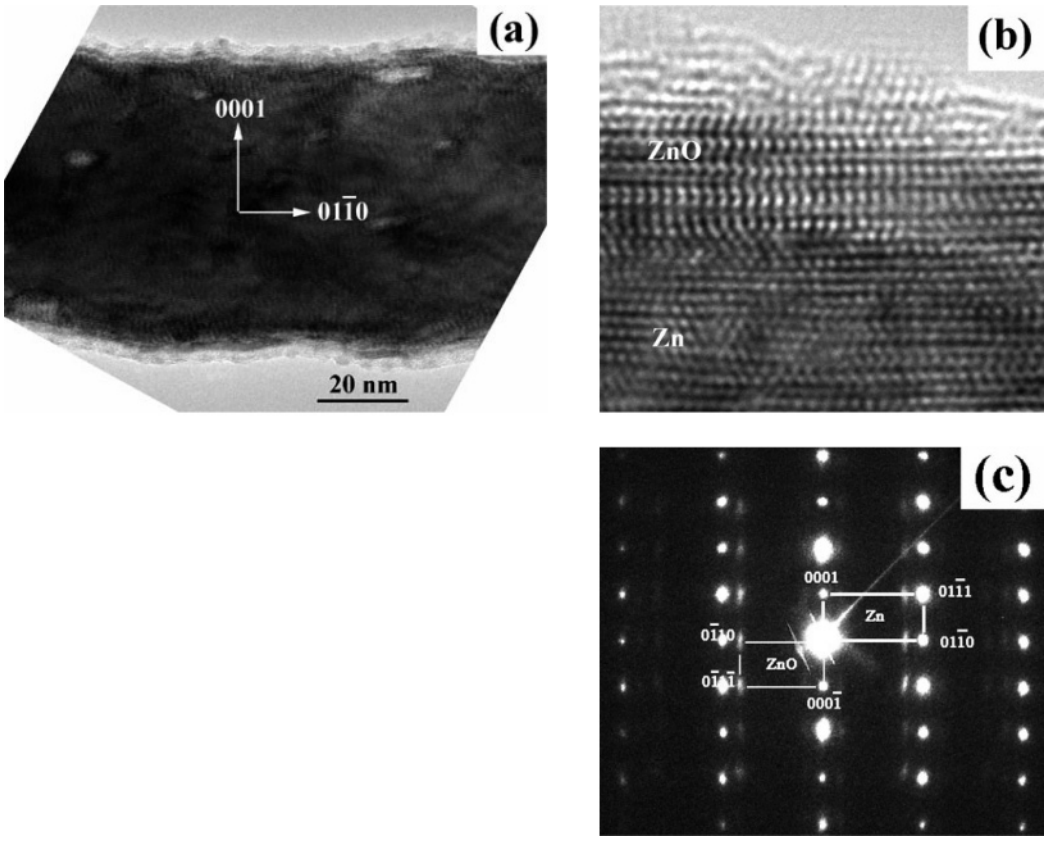

Figure 4. (a) Single-crystal nanowire growing along the [0$\bar{1}$10] direction, with the electron beam direction parallel to $[2\bar{1}\bar{1}0]_{Zn}$, (b) local enlarged HREM image of the interface between Zn and ZnO, and (c) select area electron diffraction patterns.

Figure 3 shows a single-crystal Zn nanowire with [0001] growth orientation. The electron beam direction is $[2\bar{1}\bar{1}0]_{Zn}$// $[2\bar{1}\bar{1}0]_{ZnO}$. The epitaxial relationships between Zn and the oxide layer, which could be determined from the selected area electron diffraction patterns in Figure 3c, are $[2\bar{1}\bar{1}0]_{Zn}$// $[2\bar{1}\bar{1}0]_{ZnO}$, $(0001)_{Zn}$//$(0001)_{ZnO}$. These epitaxial relationships were confirmed in the HREM images of the interface between Zn and the ZnO layer shown in Figure 3b. The mismatch along the [0001] orientation is 5.2%, which could also result in mismatch dislocations at the Zn/ZnO interface and stacking faults in the ZnO layer.

Figure 4 shows a single-crystal nanowire with [0$\bar{1}$10] growth orientation. The epitaxial relationships between Zn and the oxide layer determined from the selected area electron diffraction patterns in Figure 4c are $[2\bar{1}\bar{1}0]_{Zn}$//$[2\bar{1}\bar{1}0]_{ZnO}$, $(0\bar{1}10)_{Zn}$//$(0\bar{1}10)_{ZnO}$. Locally enlarged HREM images of the interface between Zn and the ZnO layer are shown in Figure 4b. Again, the epitaxial relationships were confirmed. There are interfacial dislocations at the Zn/ZnO interface because of the lattice mismatch between Zn and ZnO; the mismatch along the [0$\bar{1}$10] orientation is 21.6%. Similar epitaxial relationships have also been observed in Zn−ZnO core-shell nanobelts and nanotubes synthesized by a solid−vapor decomposition process.[24,25] The single-crystalline nanowires synthesized in this study have all of the three growth orientations mentioned above. At present, we do not know what the major effect to control the growth orientation is.

In contrast, Zn nanowires fabricated under condition ii, that is, at the relatively higher potential of −1.5 V and low temperature (19 °C), typically show a polycrystalline structure. An example is shown in Figure 5a. Most grains grow

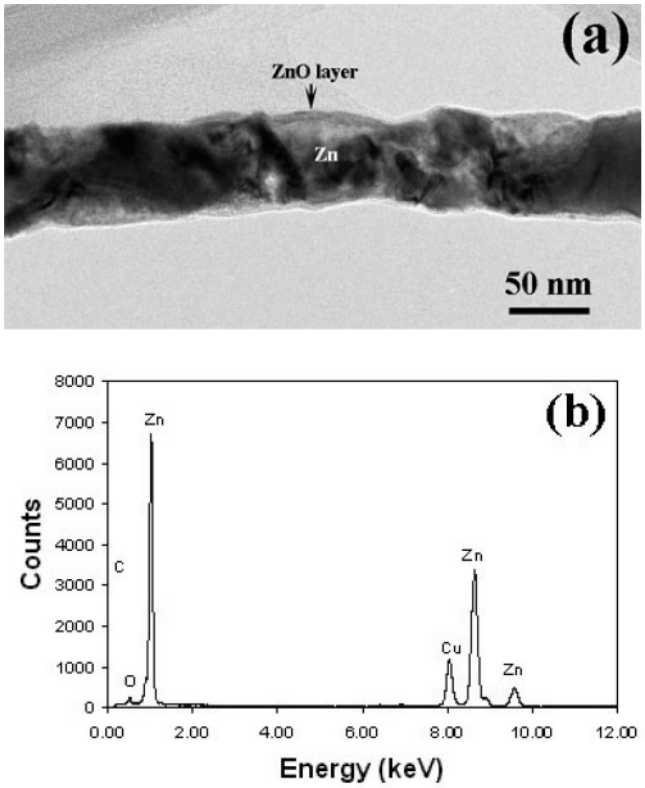

Figure 5. (a) Polycrystalline Zn nanowires synthesized with an overpotential of −1.5 V at low temperature (19 °C). (b) EDX spectrum from the wire indicated it is a metallic Zn nanowire.

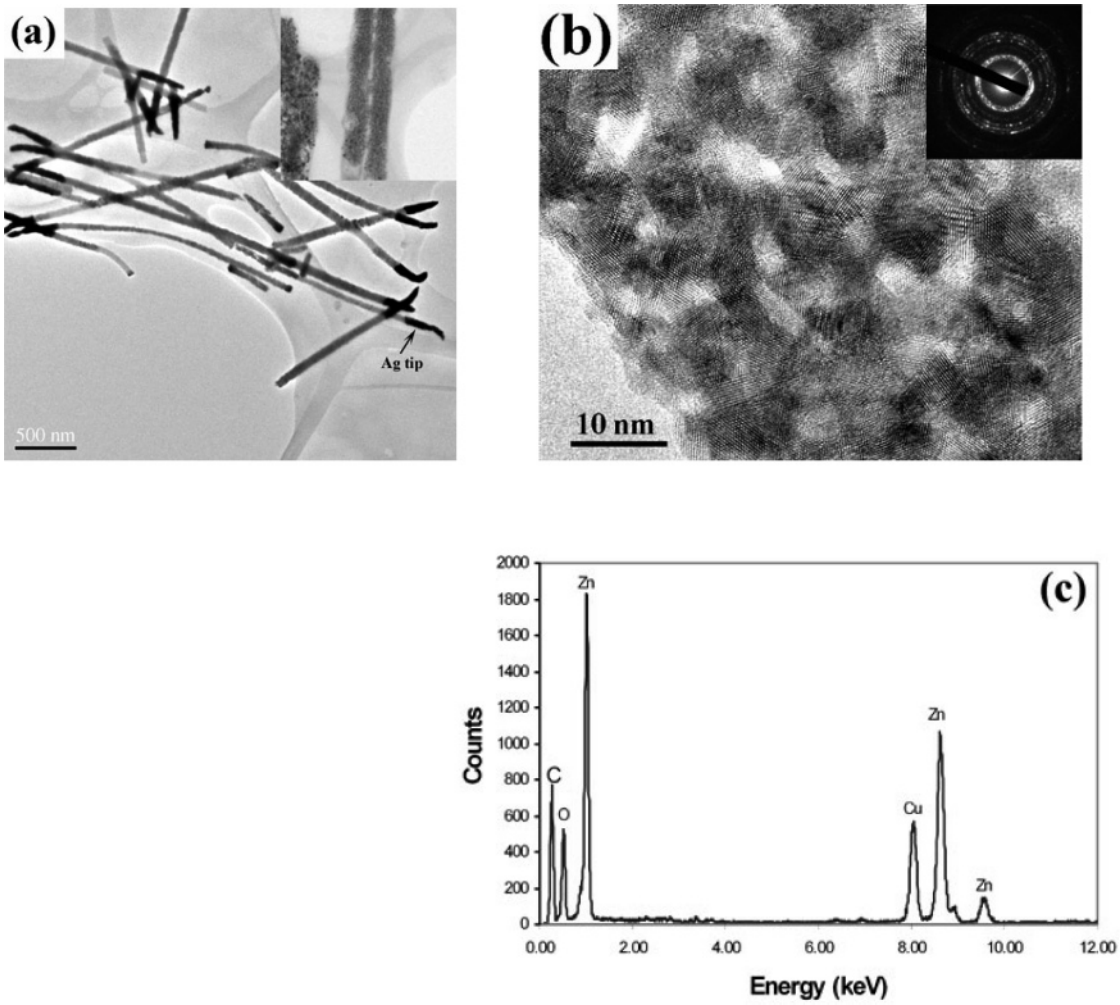

Figure 6. (a) Nanocrystalline ZnO nanowires synthesized with an overpotential of −0.7 V at low temperature (75 °C). (b) HRTEM image and electron diffraction pattern. (c) EDX spectrum from the wire indicated it is ZnO nanowire.

across the wire diameter, and the wires have a bamboolike structure. Grain boundaries are clearly observed in the wire. The EDX spectrum of the wire, which is shown in Figure 5b, indicates that the wire is metallic Zn with a ZnO layer.

Deposition under condition iii, that is, at a high temperature (75 °C) and low potential (−0.7 V), resulted in a completely nanocrystalline wire structure. Low magnification bright-field images of the nanowires are shown in Figure 6a, and a HRTEM image of a segment of a nanowire is shown in Figure 6b. The grain size is about 5 nm. The selected area electron diffraction (SAED) pattern shown in Figure 6b reveals that the nanocrystalline wires are ZnO with a hexagonal structure with lattice constants $a = 0.3249$ and $c = 0.5206$ nm, respectively. EDX analysis shown in Figure 6c confirms the SAED result. The oxide of zinc−ZnO is a versatile material used as a transparent conductor in optical devices and gas sensors; it also has potential applications in nanoelectromechanical systems.[34]

Interestingly, nanowires fabricated under condition iv, that is, at higher temperature (75 °C) and high potential (−1.5 V), show a polycrystalline Zn−ZnO composite structure, as shown in Figure 7a, in which the nanowire is composed of alternating Zn and ZnO grains. The EDX spectra from the Zn and ZnO grains were shown in Figure 7b. It is worth noting that we did not observe an epitaxial relationship between the Zn and ZnO segments of nanowires grown under these conditions. Figure 7c shows a HREM image of the interface between metallic Zn and the oxide ZnO. No apparent orientational relationship exists at the metal/metal oxide interface, and the ZnO segment is polycrystalline.

Temperature and deposition potential are known to affect the morphology, texture, grain size, and lattice defects of metallic electrodeposits.[35] In principle, a new grain will form during the electrodeposition process if the size of an initial atom cluster exceeds a critical dimension $N_c = bs\epsilon^2/(Ze\eta)^2$, where s, ϵ, Z, and η are the area occupied by one atom on the surface of the nucleus, the edge energy, the effective electron number, and the overpotential, respectively.[36] If the nucleation rate is controlled such that it is slower than the growth rate of the grain, the cluster of atoms has insufficient time to reach the critical size, N_c, and become a new nucleus. This will result in continued growth of the preexisting grain, that is, single-crystal growth. Normally, at lower deposition overpotential the nucleation rate is low and single-crystal growth is favored. With increasing deposition potential, N_c decreases and the formation of polycrystalline nanowires is favored. At low deposition temperatures, our experimental results, shown in Figures 1 and 5, qualitatively follow the

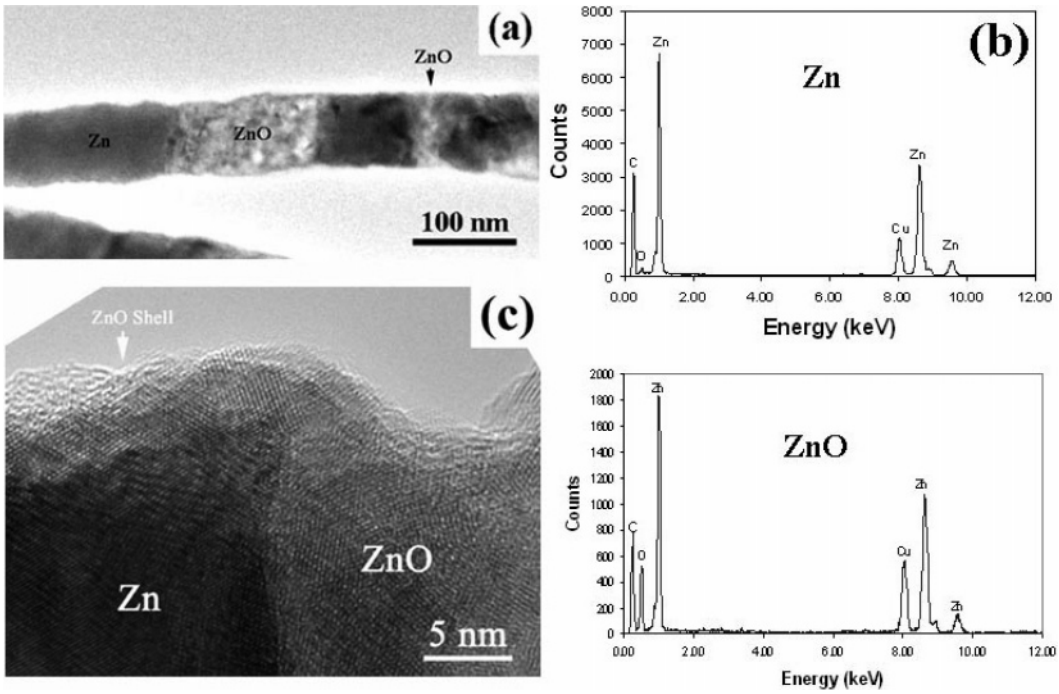

Figure 7. (a) Polycrystalline Zn−ZnO microstructure nanowire synthesized at higher temperature (75 °C) and high overpotential (−1.5 V). (b) EDX spectra from Zn and ZnO grains. (c) HRTEM image showing the Zn/ZnO grain boundary.

theoretical prediction, that is, single-crystal wires at $V_{SCE} = -0.7$ V and polycrystalline wires at −1.5 V. In both cases the as-deposited nanowires are metallic and embedded inside the membrane, and the oxidation product ZnO grows on the surface of the Zn wire after it is released from the membrane.

Slightly higher growth temperature was shown previously to favor the single-crystal growth of noble metal Ag, Au, and Cu nanowires.[29] This is because a slightly higher temperature promotes atomic diffusion on the growing face of the nanowires and thus accelerates growth relative to the nucleation of new grains. Metals with higher cohesive energy, such as Rh and Ru, grow as polycrystalline nanowires because the mobility of atoms on the metal surface is low at the accessible temperatures (<100 °C) of aqueous electrodeposition. At low growth temperature and low overpotential, Zn follows the pattern of other soft metals, forming single-crystal nanowires. However, higher temperature promotes the corrosion of electrodeposited Zn to form the stable passive phase ZnO[37] via reaction 1, which is thermodynamically spontaneous under the conditions of our experiments

$$Zn(s) + H_2O(l) = ZnO(s) + H_2(g) \quad (1)$$

At low overpotential (−0.7 V), the growth rate is slow. When the growth rate is slower than the corrosion rate, all of the Zn that is deposited is converted to ZnO and the result is a fully oxidized nanowire. At higher overpotential (−1.5 V), the deposition rate is faster than the corrosion rate, and thus a mixture of polycrystalline Zn and ZnO phases is observed in the nanowire. The competing process of metallic Zn deposition and the corrosion of newly formed Zn nuclei resulted in the formation of a Zn−ZnO composite. Because the oxidation occurs in situ during the electrodeposition process, there is no epitaxial relationship between the Zn and ZnO segments of the nanowires.

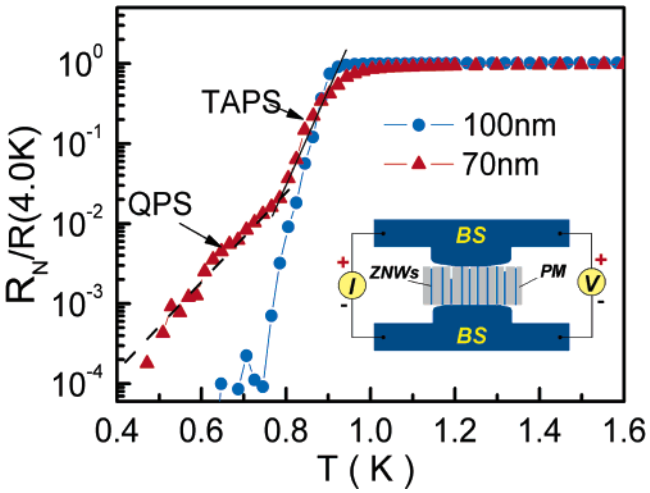

Figure 8. Normalized resistance vs temperature of 70- and 100-nm single-crystal Zn nanowires with a length of 6 μm. The inset is the schematic arrangement for our measurement.

Figure 8 shows the normalized resistance (R_N/R (4.0 K)) versus temperature (T) of 70- and 100-nm single-crystal Zn nanowires with a length of 6 μm, measured at a dc excitation current of 10 nA. The schematic arrangement of our measurement system is shown in the inset, where two superconducting In leads ($T_c = 3.4$ K) are quickly squeezed onto both sides of the membrane after the membrane is fulfilled with Zn (the details of the technique of attaching superconducting leads on nanowires have been described fully in refs 38 and 39). This excitation current is well below the critical current value (I_c) of the nanowires. Because the

series bulk In leads and the contact resistance are negligible below T_c of Zn, we are able to follow the resistance of the nanowire down to the resolution limit of our measurement system. The onset temperature, T_c, of both nanowires was found to be around 0.93 K, slightly higher than the T_c = 0.84 K of bulk Zn. However, the superconducting transition of 100-nm wires is sharp and the resistance drops to zero below 0.75 K ($\Delta T \approx 0.17$ K). In contrast, the transition of 70-nm wires broadens and shows a residual resistance extending down to 0.55 K. Two distinct linear sections are found. A high-temperature linear section is found immediately below T_c within 0.15 K. Another linear section extends from 0.77 K below T_c down to 0.55 K. The broadening of the transition near T_c in thin whiskers[40,41] and In nanowires[12] has been observed and was interpreted as a consequence of a thermally activated phase slip (TAPS) process[42,43] in a 1D syetem. The TAPS model is expected to be relevant only at temperatures very close to T_c, $\Delta T < 0.2$ K. The exponential residual resistance near T_c as shown in Figure 8 for 70-nm Zn wires is consistent with this theoretical prediction.

The second low-temperature exponential residual resistance that extends over a wide range far below T_c cannot be understood in the framework of the TAPS model. Such a finite resistance is probably from the quantum phase-slip process, suggested first by Giordano in a study of granular indium wires 41 nm in diameter, fabricated from an evaporated In film by a step-edge lithographic technique.[12,44] Our result with 70-nm Zn wires is also consistent with our previous observations of 20- and 40-nm single-crystal Sn nanowires; the only difference is that the resistive tail caused by the QPS process in Zn nanowires appears in relatively larger diameter wires. Our data indicate that 70-nm Zn wires have reached the 1D limit for quantum size confinement on superconductivity. The superconductivity of 40-nm Zn nanowires, which will be reported elsewhere, shows the strong effect of their superconducting environment.[39]

In summary, in the template synthesis of Zn nanowires, the microstructure of the nanowires can be single-crystalline or polycrystalline Zn, crystalline Zn/nanocrystalline ZnO composites, or entirely ZnO. The microstructure and composition are controlled by the deposition conditions (deposition voltage, temperature, or additives). An epitaxial relationship between Zn and ZnO was found in the single-crystalline Zn nanowires. Transport studies of single-crystal or polycrystalline Zn nanowire arrays embedded in the membranes showed that the superconducting transition temperature, T_c, is insensitive to the sample diameter and morphology. The superconductivity shows a clear crossover from bulklike to quasi-1D behavior, with residual low-temperature resistance, when the diameter of the wires is reduced to 70 nm (20 times smaller than the bulk coherence length).

Acknowledgment. This work is supported by the Penn State MRSEC funded by NSF under grant DMR-0213623.

References

(1) Bird, J. P.; Ishibashi, K.; Stopa, M.; Aoyagi, Y.; Sugano, T. *Phys. Rev. B* **1994**, *50*, 14983.
(2) Wees, B. J. v.; Kouwenhoven, L. P.; Houten, H. v.; Beenakker, C. W. J.; Mooij, J. E.; Foxon, C. T.; Harris, J. J. *Phys. Rev. B* **1988**, *38*, 3625.
(3) Wernsdorfer, W.; Doudin, B.; Mailly, D.; Hasselbach, K.; Benoit, A.; Meier, J.; Ansermet, J. P.; Barbara, B. P. R. L. *Phys. Rev. Lett.* **1996**, *77*.
(4) Whitney, T. M.; Jiang, J. S.; Searson, P. C.; Chien, C. L. *Science* **1993**, *261*, 1316.
(5) Klabunde, K. J. *Nanoscale Materials in Chemistry*; Wiley-Interscience: John Wiley & Sons: New York, 2001.
(6) Bezryadin, A.; Lau, C. N.; Tinkham, M. *Nature* **2000**, *404*, 971.
(7) Schon, G. *Nature* **2000**, *404*, 948.
(8) Arutyunov, K. Y.; Ryynänen, T. V.; Pekola, J. P.; Pavolotski, A. B. *Phys. Rev. B* **2001**, *63*, 092506.
(9) Michotte, S.; Matefi-Tempfli, S.; Piraux, L. *Appl. Phys. Lett.* **2003**, *83*, 4119.
(10) Yi, G.; Schwarzacher, W. *Appl. Phys. Lett.* **1999**, *74*, 1746−1748.
(11) Rogachev, A.; Bezryadin, A. *Appl. Phys. Lett.* **2003**, *83*, 512.
(12) (a) Giordano, N. *Phys. Rev. Lett.* **1988**, *61*, 2137. (b) Giordano, N. *Phys. Rev. B* **1990**, *41*, 6350.
(13) Giordano, N. *Phys. Rev. B* **1991**, *43*, 160.
(14) Sharifi, F.; Herzog, A. V.; Dynes, R. C. *Phys. Rev. Lett.* **1993**, *71*, 428.
(15) Lau, C. N.; Markovic, N.; Bockrath, M.; Bezryadin, A.; Tinkham, M. *Phys. Rev. Lett.* **2001**, *87*, 217003.
(16) Schulz, U.; Tidecks, R. *J. Low Temp. Phys.* **1988**, *71*, 151.
(17) Chang, S.-S.; Yoon, S. O.; Park, H. J.; Sakai, A. *Mater. Lett.* **2002**, *53*, 432−436.
(18) Yan, Y.; Liu, P.; Romero, M. J.; Al-Jassim, M. M. *J. Appl. Phys.* **2003**, *93*, 4807−4809.
(19) Peng, X. S.; Zhang, L. D.; Meng, G. W.; Yuan, X. Y.; Lin, Y.; Tian, Y. T. *J. Phys. D: Appl. Phys.* **2003**, *36*, L35−L38.
(20) Wang, Y.; Zhang, L.; Meng, G.; Liang, C.; Wang, G.; Sun, S. *Chem. Commun.* **2001**, *24*, 2632−2633.
(21) Wu, J.-J.; Liu, S.-C.; Wu, C.-T.; Chen, K.-H.; Chen, L.-C. *Appl. Phys. Lett.* **2002**, *81*, 1312−1314.
(22) Hu, J. Q.; Bando, Y.; Liu, Z. W. *Adv. Mater.* **2003**, *15*, 1000−1003.
(23) Hu, J. Q.; Li, Q.; Meng, X. M.; Lee, C. S.; Lee, S. T. *Chem. Mater.* **2003**, *15*, 305−308.
(24) Kong, X. Y.; Ding, Y.; Wang, Z. L. *J. Phys. Chem. B* **2004**, *108*, 570−574.
(25) Ding, Y.; Kong, X. Y.; Wang, Z. L. *J. Appl. Phys.* **2004**, *95*, 306−310.
(26) Martin, C. R. *Science* **1994**, *266*, 1961−1966.
(27) Huczko, A. *Appl. Phys. A* **2000**, *70*, 365−376.
(28) Martin, C. R. *Chem. Mater.* **1996**, *8*, 1739−1746.
(29) Tian, M. L.; Wang, J. G.; Kurtz, J.; Mallouk, T. E.; Chan, M. H. W. *Nano Lett.* **2003**, *3*, 919.
(30) Tian, M. L.; Wang, J. G.; Snyder, J.; Kurtz, J.; Liu, Y.; Schiffer, P.; Mallouk, T. E.; Chan, M. H. W. *Appl. Phys. Lett.* **2003**, *83*, 1620−1622.
(31) Wang, J. G.; Tian, M. L.; Mallouk, T. E.; Chan, M. H. W. *J. Phys. Chem. B* **2004**, *108*, 841−845.
(32) Wang, J. G.; Tian, M. L.; Mallouk, T. E.; Chan, M. H. W. *Nano Lett.* **2004**, *4*, 1313.
(33) Sun, H.; Pan, X. *J. Mater. Res.* **2004**, *19*, 3062−3067.
(34) Kong, X. Y.; Wang, Z. L. *Nano Lett.* **2003**, *3*, 1625−1631.
(35) Budevski, E.; Staikov, G.; Lorenz, W. J. *Electrochim. Acta* **2000**, *45*, 2559.
(36) Paunovic, M.; Schlesinger, M. *Fundamentals of Electrochemical Deposition*; Wiley: New York, 1998.
(37) Beverskog, B.; Puigdomenech, I. *Corros. Sci.* **1997**, *39*, 107−114.
(38) Tian, M. L.; Wang, J. G.; Kurtz, J. S.; Liu, Y.; Mayer, T. S.; Mallouk, T. E.; Chan, M. H. W. *Phys. Rev. B* **2005**, *71*,104521.
(39) Tian, M. L.; Kumar, N.; Xu, S. Y.; Wang, J. G.; Kurtz, J. S.; Chan, H. W. M. *Phys. Rev. Lett.*, submitted for publication, 2005.
(40) Lukens, J. E.; Warburton, R. J.; Webb, W. W. *Phys. Rev. Lett.* **1970**, *25*, 1180.
(41) Newbower, R. S.; Beasley, M. R.; Tinkham, M. *Phys. Rev. B* **1972**, *5*, 864.
(42) Langer, J. S.; Ambegaokar, V. *Phys. Rev.* **1967**, *164*, 498.
(43) McCumber, D. E.; Halperin, B. I. *Phys. Rev. B* **1970**, *1*, 1054.
(44) Giordano, N. *Phys. Rev. B* **1980**, *22*, 5635.

NL050918U